

Self-Assembly of Giant Mo_{240} Hollow Opening DodecahedraJiaomin Lin,[#] Ning Li,[#] Shiping Yang,^{*} Mingjie Jia, Jiang Liu,^{*} Xiao-Min Li, Lu An, Qiwei Tian, Long-Zhang Dong, and Ya-Qian Lan^{*}Cite This: *J. Am. Chem. Soc.* 2020, 142, 13982–13988

Read Online

ACCESS |



Metrics & More

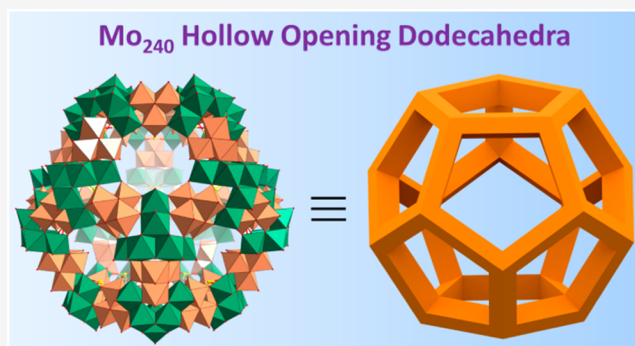


Article Recommendations



Supporting Information

ABSTRACT: The synthesis of hollow opening polyhedral cages has always been an attractive but challenging goal, especially with regard to inorganic polyhedral cages. Herein, we present a novel, 240-nuclearity giant polymolybdate cage prepared via hydrothermal synthesis. This cage is composed of 20 tripod-shaped $[\text{Mo}_6\text{O}_{22}(\text{SO}_3)]^{n-}/[\text{Mo}_6\text{O}_{21}(\text{SO}_4)]^{n-}$ building blocks with three connected vertices and 30 cubane-type $[\text{Mo}_4\text{O}_{16}]^{n-}$ edge building blocks, featuring a rare, nearly regular pentagonal dodecahedron with a large inner cavity (diameter up to 1.8 nm) and 12 opening pentagonal windows. This is the highest nuclearity hollow opening dodecahedral cage reported to date. Importantly, this cage exhibits good stability in solution, as revealed by scanning transmission electron microscopy (STEM), TEM, UV-vis, and Raman spectra. In addition, the bulk sample of this compound exhibits an ultrahigh proton conductivity of $1.03 \times 10^{-1} \text{ S cm}^{-1}$ at 80 °C and 98% relative humidity, which is the highest among polyoxometalate-based crystalline proton conductors.



INTRODUCTION

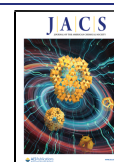
Hollow opening polyhedral cages have attracted considerable attention because of their aesthetic architectures and interesting application in catalysis, guest encapsulation, adsorption/separation, and ion/proton transportation.^{1–8} Of the available polyhedral prototypes, Platonic bodies whose faces consist of only one single, regular polygon are particularly attractive geometric entities.¹ Various hollow opening polyhedral cages with the shapes of small Platonic polyhedra such as tetrahedrons, cubes, and octahedrons have been constructed via different assembly strategies such as edge- and face-directed self-assembly.^{1–3} Their well-defined single-crystal structures in turn guide the design and synthesis of diverse cage-based materials with desired architectures and properties.^{2–4} In contrast, hollow opening cages with pentagonal dodecahedron architecture (the largest Platonic polyhedron with I_h symmetry) are rarely observed,^{9–13} although an edge-directed assembly approach for the synthesis of such polyhedral cages was developed by Stang et al. in 1999.⁹ Indeed, construction of a pentagonal dodecahedron typically requires self-assembly of 20 tripodal secondary building blocks (SBBs) with angle of $\sim 108^\circ$ (as vertices) and 30 ditopic SBBs with angle of $\sim 180^\circ$ (as edges).⁹ This is substantially more difficult than constructing other small Platonic polyhedra. In addition, maintaining the structural stability of such a hollow opening polyhedral cage is often quite challenging due to its large volume. Thus, single-crystal prototype structures of dodecahedral cages, especially those that have geometries

approaching the ideal pentagonal dodecahedrons, are still exceedingly rare.^{10–13}

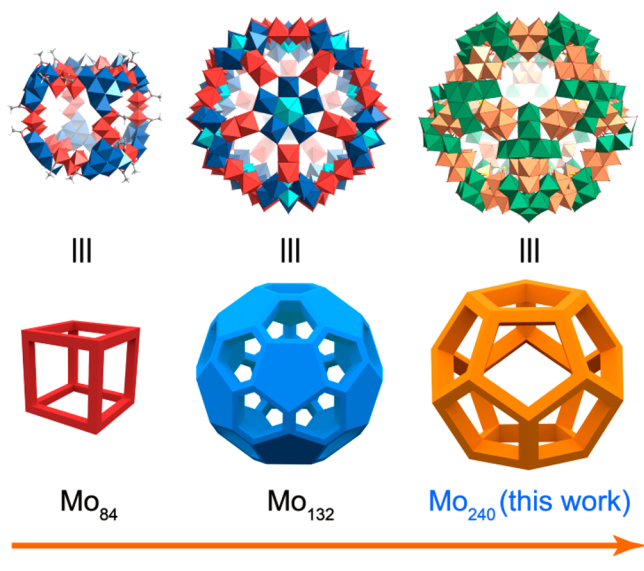
Polyoxometalates (POMs) that assemble from early transition metal oxides with rich physicochemical properties are well-known, alluring SBBs for constructing various all-inorganic/inorganic–organic hybrid hollow opening cages or polyhedral cages.^{14–19} For example, several famous giant hollow opening cages (including polyhedral cages, Scheme 1), such as “hedgehog-like” Mo_{368} ,²⁰ wheel-shaped Mo_{248} ,²¹ truncated icosahedral Mo_{132} ,²² truncated icosahedral U_{60} ,²³ and box-shaped Mo_{84} ,²⁴ have been achieved using different POM SBBs. These giant hollow opening POM cages not only provide intriguing structures but also combine the benefits of POM clusters (e.g., their anionic nature and redox activities) and molecular cages (e.g., well-defined windows and cavities) and thus are highly promising for applications in selective catalysis, ion transport, and proton conductivity.^{8,25–28} Nevertheless, it still remains a great synthetic challenge to explore new architectures to enrich the topological structures of this giant POM-cage family. In particular, the hollow opening giant polyhedral cages with high symmetry and high nuclearity are still rarely reported. This is probably because of the high

Received: June 18, 2020

Published: July 21, 2020



Scheme 1. Structures and Polyhedral Geometries of the Reported Representative High-Nuclearity Hollow Opening Giant Polymolybdate Polyhedral Cages Mo_{84} and Mo_{132} , and Cage 1



requirements for their hollow opening polyhedron construction and large nuclearity growth, since their formations usually require the orderly self-assembly (in space) of a great number of small metal-oxo SBBs, which however instinctively tend to form nonporous structures during self-assembly.

In this paper, a hollow opening dodecahedral POM cage with a formula of $(\text{NH}_4)_{21}\text{H}^{+}_{59-2x}[\text{Mo}^{\text{V}}_{180}\text{Mo}^{\text{VI}}_{60}(\text{OH})_{60}\text{O}_{620-x}(\text{SO}_3)_{20-x}(\text{SO}_4)_x]\cdot\text{ca}337\text{H}_2\text{O}$ (denoted as

$\text{Mo}_{240}\cdot\text{g}$ or **1·g**) is synthesized via a solvothermal reaction. The structure of this cage has two remarkable features: (1) it is built by two kinds of polymolybdate SBBs and contains 1000 non-hydrogen atoms per molecular cluster, including 240 Mo, 740 O, and 20 S atoms and (2) it has nearly regular pentagonal dodecahedral geometry with a 1.8 nm inner cavity and 12 open pentagonal windows. With these unique structural features, cage **1** is by far the highest nuclearity hollow opening dodecahedral cage (currently reported hollow opening dodecahedrons including inorganic cages: U_{20} ¹⁰ and $\text{Sn}_{36}\text{Ge}_{24}$ ¹¹ and inorganic–organic hybrid cages: Pt_{20} ,⁹ U_{20} ,¹² and Co_{20} ¹³). Furthermore, cage **1** shows high stability in solution and can be visualized by scanning transmission electron microscopy (STEM) and transmission electron microscopy (TEM) imaging. In addition, the bulk conductivities of **1·g** reached $3.33 \times 10^{-2} \text{ S cm}^{-1}$ at 25 °C and 98% relative humidity (RH) and $1.03 \times 10^{-1} \text{ S cm}^{-1}$ at 80 °C and 98% RH, respectively, representing the highest among the reported POM-based crystalline proton conductors under the analogous conditions.^{27,29–35}

RESULTS AND DISCUSSION

A dark red, polygonal crystal of **1·g** was synthesized via a hydrothermal reaction between $(\text{NH}_4)_6\text{Mo}_7\text{O}_{24}$, CoSO_4 and $\text{NH}_2\text{NH}_2\cdot 2\text{HCl}$ in H_2O in the presence of trace, dilute H_2SO_4 (Figure S1). The CoSO_4 can be replaced with another sulfate such as FeSO_4 , MnSO_4 , CuSO_4 , or ZnSO_4 . The structure and elemental composition of **1·g** were determined by single-crystal X-ray diffraction and various other analytical techniques. In this reaction, SO_3^{2-} anions should be generated in situ via reduction of SO_4^{2-} anions by $\text{NH}_2\text{NH}_2\cdot 2\text{HCl}$ during the hydrothermal reaction. We attempted to replace the sulfate

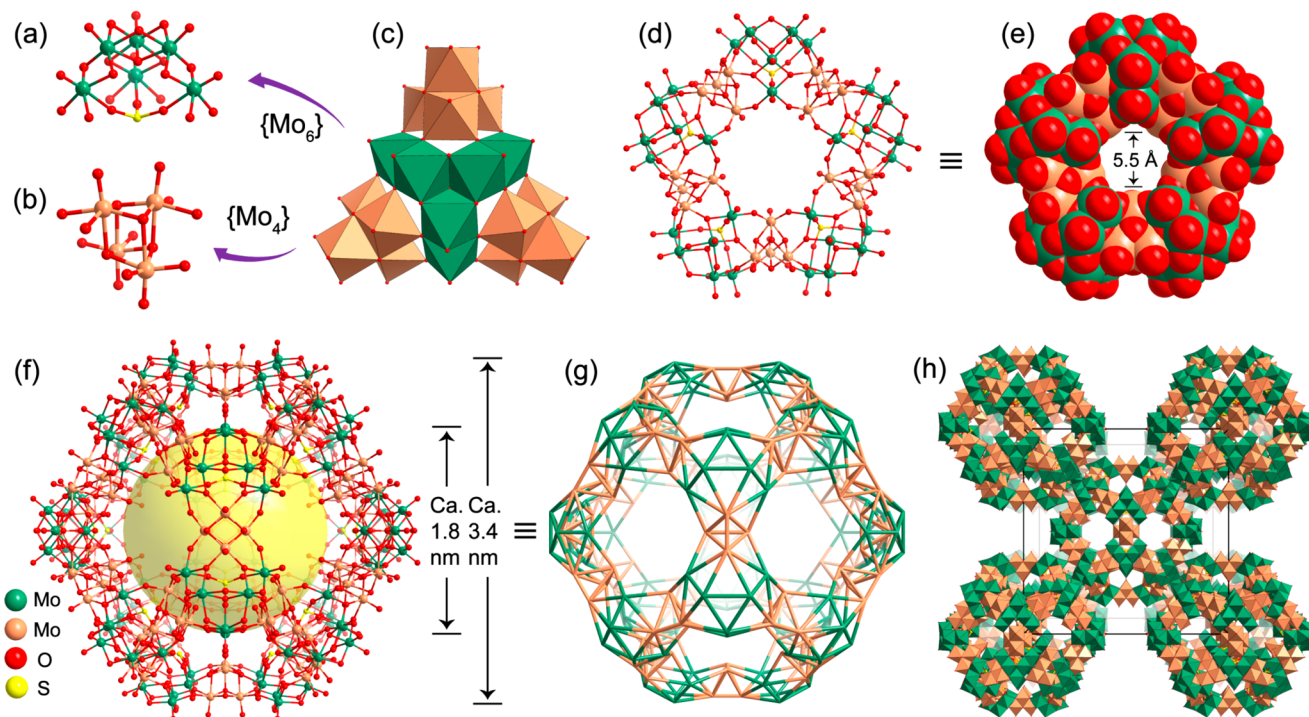


Figure 1. Crystal structure of dodecahedral cage **1**. (a) The $\{\text{Mo}_6\}$ and (b) $\{\text{Mo}_4\}$ secondary building blocks and (c) the connection between $\{\text{Mo}_6\}$ and $\{\text{Mo}_4\}$. (d) Ball-and-stick and (e) space-filling views of the pentagonal window. (f) Ball-and-stick view of the structure of **1**. (g) Metal atom-based skeleton of **1** in ball-and-stick representation. (h) The body-cubic packing of **1** in polyhedral representation. Polyhedra code: $\{\text{Mo}_6\}$, green; $\{\text{Mo}_4\}$, tan.

with Na_2SO_3 , but **1**·**g** was not obtained, indicating that the in situ generated SO_3^{2-} ligand may be crucial to **1**·**g** formation.

Crystallographic structure analysis revealed that compound **1**·**g** crystallizes in the cubic space group $Im\bar{3}$ (Figure S2 and Table S1). The skeleton of **1** can be considered as an assembly of 20 $[\text{Mo}_6\text{O}_{22}(\text{SO}_3)]^{n-}/[\text{Mo}_6\text{O}_{21}(\text{SO}_4)]^{n-}$ (denoted as $\{\text{Mo}_6\}$) SBBs and 30 $[\text{Mo}_4\text{O}_{16}]^{n-}$ (denoted as $\{\text{Mo}_4\}$) SBBs. This skeleton features a hollow opening dodecahedral structure with T_h symmetry (Figure 1).

Each $\{\text{Mo}_6\}$ SBB is built up by three dumbbell-shaped $\{\text{Mo}_2\}$ units and a SO_3^{2-} or SO_4^{2-} anion (Figure 1a and Figure S2). The three $\{\text{Mo}_2\}$ units form a tripod-shaped configuration by sharing three edges and a common vertex. Each tripod-shaped $\{\text{Mo}_6\}$ SBB contains either a pyramidal $\mu_3\text{-}\eta^1\text{:}\eta^1\text{:}\eta^1\text{-}\text{SO}_3^{2-}$ anion at its chassis or a tetrahedral $\mu_6\text{-}\eta^3\text{:}\eta^1\text{:}\eta^1\text{:}\eta^1\text{-}\text{SO}_4^{2-}$ anion in its center (Figure S3). The $\{\text{Mo}_6\}$ SBB can also be described as a lacunary ϵ -Keggin polymolybdate since its structure is similar to that of the classic ϵ -Keggin-type core $[\text{XMo}_{12}\text{O}_{40}]^{n-}$ ($\text{X} = \text{S}, \text{P}, \text{Si}, \text{or Ge}$) with six coplanar MoO_6 octahedra removed (Figure S4). For the whole structure of **1**, the 20 $\{\text{Mo}_6\}$ SBBs can be divided into two groups. Twelve of the SBBs are located at the mirror plane and contain SO_3^{2-} in the chassis or SO_4^{2-} in the center (the SO_3^{2-} and SO_4^{2-} anions are in crystallographic disorder), and eight are located at the C_3 symmetric axis with SO_3^{2-} anions in the chassis. The SO_3^{2-} anion with trigonal–pyramidal configuration may generate substantial steric hindrance for preventing $\{\text{Mo}_6\}$ SBB from forming the saturated ϵ -Keggin $[\text{XMo}_{12}\text{O}_{40}]^{n-}$ core and thus behaves as a crucial ligand for the formation of the $\{\text{Mo}_6\}$ SBB. Bond valence sum calculations (BVSs) show that all Mo centers in the $\{\text{Mo}_6\}$ SBB are in the + V oxidation state (Tables S2–S3). The Mo···Mo distances in each $\{\text{Mo}_2\}$ unit are in the range of 2.63(1)–2.64(1) Å, which corresponds to a Mo–Mo single bond.

Unlike the $\{\text{Mo}_6\}$ SBB, the $\{\text{Mo}_4\}$ SBB consists of one dumbbell-shaped $\{\text{Mo}_2\}$ unit and two $\{\text{Mo}_1\}$ units, which form a cubane-type structure by sharing six edges (Figure 1b). BVS calculations show that the oxidation states of the Mo centers in the $\{\text{Mo}_2\}$ unit are + V, whereas those in the $\{\text{Mo}_1\}$ unit are + VI (Table S2). This indicates that the $\{\text{Mo}_4\}$ SBB is a mixed-valence cluster. Aside from the $\{\text{Mo}_2\}$ unit that forms a Mo–Mo single bond of 2.639(2) Å, the other intracubane Mo···Mo distances are in the range of 3.195(2)–3.394(2) Å. The 30 $\{\text{Mo}_4\}$ SBBs can also be divided into two groups. Six of the SBBs are located in the C_2 symmetric axis, and 24 are positioned at the glide plane.

The $\{\text{Mo}_6\}$ and $\{\text{Mo}_4\}$ SBBs are linked together by $\mu_2\text{-O}$ and $\mu_3\text{-O}$ bridges (Mo–O bands, 1.801(1)–2.092(1) Å) to form the titled giant polymolybdate cage **1** with dimensions of ca. $3.4 \times 3.4 \times 3.4$ nm (Figures 1c, 1f, and S5). The overall skeleton of **1** contains 240 molybdenum, 740 oxygen, and 20 sulfur atoms. Thus, 1000 atoms are involved in the formation of this giant polymolybdate cage (Figure S6). Of the reported giant polymolybdate clusters, only a few examples such as Mo_{248}^{21} and Mo_{368}^{20} contain over 200 molybdenum atoms and over 1000 total atoms.

If each $\{\text{Mo}_6\}$ SBB is viewed as a tritopic vertex and each $\{\text{Mo}_4\}$ SBB is viewed as a ditopic edge, cage **1** can be simplified as a pentagonal dodecahedron with 20 vertices and 12 pentagonal faces (Figure S7). Note that clusters that exhibit pentagonal dodecahedral geometry are also named as fullerene-like clusters, which have attracted considerable attention over recent decades because of their unique structures and

properties.³⁶ Nevertheless, many of the reported fullerene-like inorganic clusters possess (multi)-shell-like structures and hence typically do not exhibit large cavities or windows.³⁶ In contrast, this giant dodecahedral cage has a large inner cavity connected to 12 open pentagonal windows (Figure 1f, 1g). The free diameter of the cavity is approximately 1.84 nm, and the void volume is about 3260 Å³. These parameters are comparable to those of the famous Mo_{132} (diameter and void volume of 1.86 nm and 3368 Å³, respectively).²² The cavity was occupied by disordered solvent molecules and counterions, which however are difficult to be modeled. Each pentagonal window is composed of 10 MoO_6 octahedra (Figure 1d) and has a diameter of approximately 5.5 Å (Figure 1e and Figure S8), which is big enough for diffusion of some small guest molecules (e.g., H_2O). In the crystal lattice, cage **1** packs in an orderly, body-cubic arrangement, resulting in small tunnels along the crystallographic axes (Figure 1h).

To improve our understanding of the geometric structure of this giant POM cage, we built a pentagonal dodecahedron by connecting each common vertical O atom of the 20 $\{\text{Mo}_6\}$ SBBs (Figure 2a). This pentagonal dodecahedron is amazingly

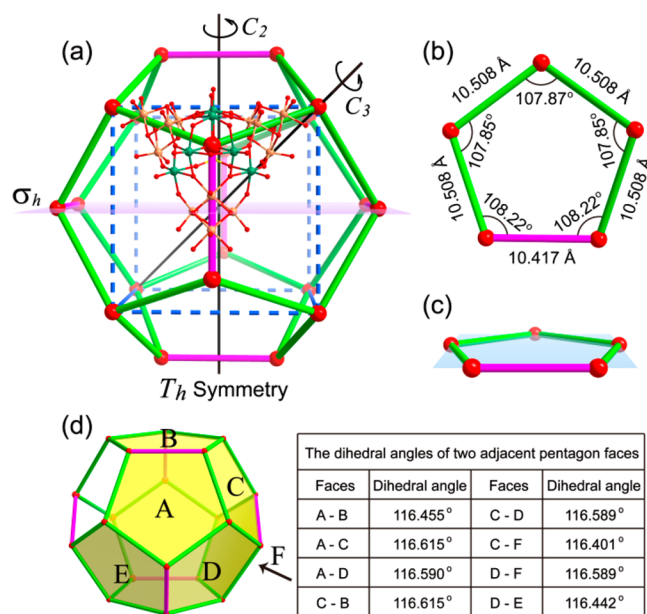


Figure 2. (a) Dodecahedral cage formed by connecting each common vertical O atom of the 20 $\{\text{Mo}_6\}$ vertices. In the inset, a regular cube (blue dotted line) inside the dodecahedron forms from the 8 $\{\text{Mo}_6\}$ vertices located at the C_3 axis. (b) Pentagon window and its edge lengths (vertex–vertex O···O distance) and inner angles. The four isometric edges are shown as green bonds, and the other is shown as a pink bond. (c) Side view of the pentagon, showing that the five vertices are nearly coplanar. (d) The dihedral angles between two adjacent pentagons in the dodecahedron.

regular and has T_h symmetry similar to that of the metallo-carbocubane Ti_8C_{12} .³⁷ As shown in Figure 2b, each pentagon of the dodecahedron contains four edges with lengths of 10.508 Å (vertex–vertex O···O distance) and one edge with a length of 10.417 Å, which is nearly the same. Moreover, the vertex O atoms that define each pentagon are nearly coplanar (Figure 2c) since the perpendicular deviations of the vertex O atoms from the mean plane are only -0.004 to $+0.024$ Å. The inner pentagon angles are 107.85° – 108.22° (Figure 2b), and the dihedral angles of each adjacent pentagon pair are in the

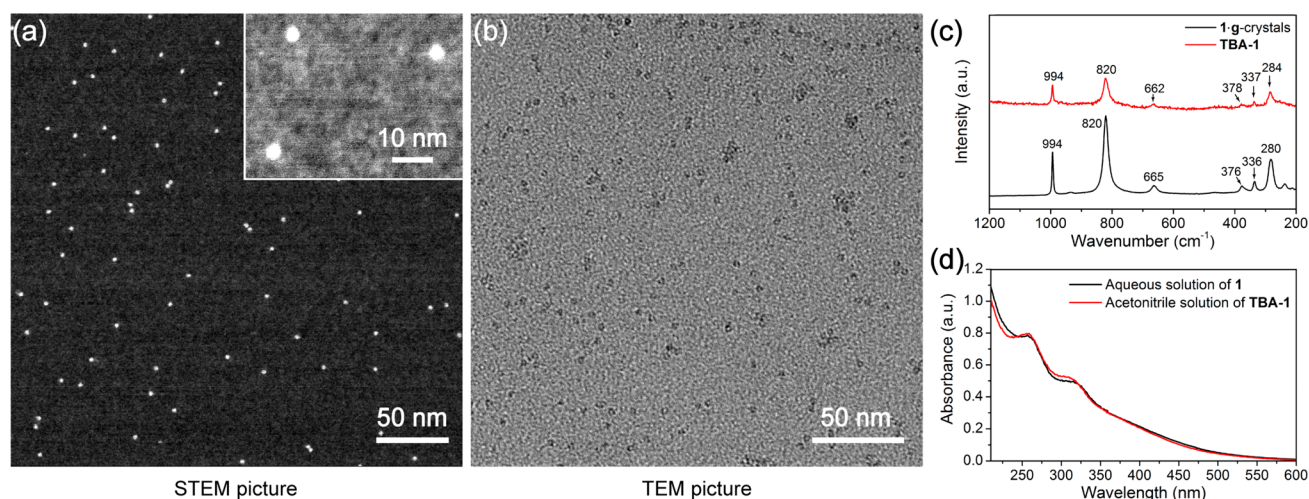


Figure 3. (a) Dark-field STEM and (b) TEM images of TBA-1. The inset image is the high-magnification STEM image. (c) Raman spectra of the crystal sample of **1-g** and TBA-1. (d) UV-vis absorption spectra of **1** in H₂O and TBA-1 in acetonitrile.

range of 116.40°–116.62° (Figure 2d). These angles are quite similar to the 108° and 116.57°, respectively, encountered in a regular pentagonal dodecahedron with perfect I_h symmetry. In addition, eight vertex O atoms from the {Mo₆} SBBs located at the C₃ axis form a regular inner cube, in which each edge length is 16.987 Å (Figure 2a). The rates of the edge lengths between the dodecahedron and the inner cube are 0.613–0.619, which are close to the ideal golden ratio of 0.618 for a regular dodecahedron. Therefore, cage **1** may be regarded as a nearly regular pentagonal dodecahedron, although its symmetry is T_h .

Hollow opening dodecahedral cages remain an attractive synthetic target, albeit very challenging because of their high symmetry, complex geometric structures, and large volume. To obtain their crystal structures is usually more challenging. To date, only a few relatively low nuclearity and symmetry hollow opening dodecahedral cages, including U₂₀ (C_{2h}),¹⁰ [Sn₃₆Ge₂₄Se₁₃₂]²⁴⁻ (C_i),¹¹ [U₂₀O₄₀L₁₂] (D_{2h}) (L = 25,26,27,28,29-pentahydroxycalix[5]arene-5,11,17,23,29-pentacarboxylic acid),¹² and [Co₂₀L₁₂(OH)₁₂(H₂O)₄]·8BF₄⁻·guest (T) (**1**, H₂L1 = 1,3-bis[(2-methyl-1*H*-imidazol-4-yl)methyleneaminomethyl]-benzene and 2 H₂L2 = 1,3-bis[(2,5-dimethyl-1*H*-imidazol-4-yl)methyleneaminomethyl]-benzene),¹³ have been achieved with well-defined crystal structures (Figure S9). To the best of our knowledge, cage **1** is the highest nuclearity and symmetry hollow opening dodecahedra synthesized thus far. Moreover, the size of cage **1** is much larger than that of the other two inorganic cages U₂₀ and [Sn₃₆Ge₂₄Se₁₃₂]²⁴⁻ and comparable to that of [U₂₀O₄₀L₁₂] constructed by inorganic nodes and large organic ligands.

With high nuclearity and large hollow opening dodecahedral geometry, cage **1** can be regarded as a new member of the giant polymolybdate cage family (Figure S10). Interestingly, for the famous polymolybdate cages, such as Mo₁₃₂²² and Mo₃₆₈,²⁰ their skeletons are mainly built using pentagonal {Mo(Mo₅)} as 5-connected faces and {Mo₂} or {Mo₁} as edges, showing homogeneous distribution of the metal centers, while for cage **1**, it is built using tripod-shaped {Mo₆} as vertices and cubane-shaped {Mo₄} as edges, displaying uneven distribution of the Mo centers (Figure S10).

The phase purity of **1-g** was confirmed by power XRD analysis (Figure S11). Elemental mapping images reveal

uniform distributions of Mo, O, and S in the crystal of **1-g**. This is also verified via energy-dispersive X-ray spectroscopy (EDS) spectra (Figure S12). The FT-IR spectrum of **1-g** exhibits characteristic bands at 959 cm⁻¹, 748 cm⁻¹, and 560 cm⁻¹, which should be attributed to stretching vibrations of terminal Mo=O bands, antisymmetric stretching vibrations of Mo–O–Mo bridges, and bending vibrations of Mo–O–Mo bridges, respectively (Figure S13).²⁷ The peaks at 972 and 1166 cm⁻¹ are assigned to the stretching vibrations of S–O in SO₃²⁻ and SO₄²⁻, respectively, which are similar to those observed in other SO₃²⁻- and SO₄²⁻-centered POM clusters.^{38,39} The Raman spectrum of **1-g** features strong peaks at 994 and 820 cm⁻¹ from the vibrations of terminal Mo=O bands and Mo–O–Mo bridges, respectively (Figure S14).⁴⁰ The high-resolution X-ray photoelectron spectrum (XPS) of Mo in **1-g** could be fitted to four peaks at 236.0, 235.3, 232.8, and 232.1 eV, which correspond to the binding energies of Mo(VI)-3d_{3/2}, Mo(V)-3d_{3/2}, Mo(VI)-3d_{5/2}, and Mo(V)-3d_{5/2}, respectively, thus demonstrating that the valence states of Mo atoms in **1** are +V and +VI (Figure S15).⁴¹ The high-resolution XPS of the S 2p spectrum displays two peaks at 164.6 and 169.3 eV with area ratio of 11/9 (Figure S16). The peaks at 164.6 and 169.3 eV corresponded to the S 2p binding energies of the S⁴⁺ and S⁶⁺ for the SO₃²⁻ and SO₄²⁻ in **1-g**, respectively.^{42,43} Thermogravimetric analysis (TGA) reveals that **1-g** exhibits about 14.4% weight loss between approximately 25 and 250 °C (Figure S17). This corresponds to approximately 337 H₂O molecules per cage, suggesting that **1** is a hydrophilic cage. This is also verified by H₂O vapor sorption measurement at room temperature. As shown in Figure S18, the H₂O vapor sorption isotherm of **1** exhibits a sigmoidal shape with a moderate hysteresis loop at P/P₀ = 0.2. The total uptake is 99 cm³ g⁻¹ at P/P₀ = 0.2 and reaches 212 cm³ g⁻¹ at P/P₀ = 0.99, demonstrating that **1** is a hydrophilic, porous cage.

The stability of cage **1** was characterized by STEM, TEM, UV-vis, and Raman spectra. Because compound **1** is almost insoluble in most common organic solvents (e.g., ethanol, acetonitrile, and acetone) and displays limited solubility in H₂O, it tends to aggregation upon H₂O evaporation, and we prepared a tetrabutylammonium (TBA) salt of **1** (denoted as TBA-1) that has good solubility in acetonitrile and acetone for

preparing monodispersed cages of **1** on a silicon chip for STEM and TEM imaging (Figure S19). Briefly, a diluted aqueous solution of **1** was mixed with an aqueous solution of tetrabutylammonium bromide and then centrifuged to obtain brown precipitation of TBA-**1** (Figure S19). A dilute solution of TBA-**1** in acetonitrile was loaded onto a silicon chip, and after the acetonitrile was evaporated under ambient atmosphere, the silicon chip was used for STEM and TEM imaging. As shown in Figure 3a and Figure S20, identifiable uniform bright dots with size of 3.2 ± 0.2 nm could be observed in the dark-field STEM image. The size of the bright dots compares well with the core size of cage **1**. In addition, the individual core of cage **1** could also be observed in the TEM image (Figure 3b and Figure S20), suggesting that the structure of this high nuclearity opening dodecahedral cage has good stability in H₂O and acetonitrile solution. This is also confirmed by Raman and UV-vis spectra. As shown in Figure 3c, the Raman spectrum of TBA-**1** exhibits similar scattering peaks to the crystal sample of **1**·g, indicating that the structure of **1** was maintained during the preparation of TBA-**1**. Moreover, UV-vis absorption spectra of **1** in aqueous solution and TBA-**1** in acetonitrile solution exhibit consistent absorptions at about 257 and 312 nm (Figure 3d), and their absorption profiles remain almost unchanged for 3 days (Figure S21), confirming the good stability of cage **1** in H₂O and acetonitrile solution.

The presence of rich H₂O molecules, terminal oxygen atoms, and counter cations (e.g., H⁺, NH₄⁺, N₂H₅⁺/N₂H₆²⁺) within the hydrophilic, porous cage **1** suggests that it may be a good proton conductor candidate.^{27,29,30} Alternating current (AC) impedance measurements of the synthesized crystalline powder sample in compacted pellets were performed at 25 °C and RH values of 40–98%. The bulk conductivity was determined based on the semicircles in the Nyquist plots. As presented in Figure 4a, at 25 °C and 40% RH, **1** exhibits a moderated proton conductivity of 2.04×10^{-6} S cm⁻¹. The proton conductivity increases rapidly with the increasing RH (Figure 4b). At 25 °C and 98% RH, the proton conductivity of **1** reaches a maximum of 3.33×10^{-2} S cm⁻¹, which is significantly higher than most known POM-based crystalline

proton conductors under analogous conditions (Table S4).^{27,29–35} The highly humidity-dependent proton conductivity implies that the water molecules play a significant role in conduction and that protons migrate primarily inside and outside of pores and channels in **1**.^{30,31,44} As demonstrated by the room-temperature H₂O vapor sorption measurement (Figure S18), **1** has an outstanding water uptake capacity under high humidities. This may facilitate the construction of hydrogen bond networks that can act as proton transport pathways within the channels of **1**, thus leading to outstanding conductivity.^{30,31,44}

The proton conductivity was further examined by increasing the temperature from 25 to 80 °C under a constant RH of 98%. As shown in Figure 4c, the proton conductivity increases with the increasing temperature. This should be attributed to possible promotion of H₃O⁺ ion formation (from H₂O and H⁺) at elevated temperatures and thus accelerate the proton transition within the channels.^{30,31,44} At 80 °C and 98% RH, the proton conductivity reaches 1.03×10^{-1} S cm⁻¹, which is the highest among the reported crystalline, POM-based proton conductors (Table S4)^{27,29–35} and comparable to those of the high-performing metal–organic (MOF) and covalent–organic (COF) frameworks.^{30,31,44–48} Indeed, there are only a few MOFs and COFs, including BUT-8(Cr)A,⁴⁵ PCMOF2_{1/2}(Tz or Pz),⁴⁶ IM-UiO-66-AS,⁴⁷ and H₃PO₄@COFs,⁴⁸ with proton conductivities on the order of 10⁻¹ S cm⁻¹ under analogous conditions (Table S4). To investigate the conductivity stability of **1**, the proton conductivity was monitored for 24 h at 80 °C and 98% RH, and negligible change was noted (Figure S22). In addition, the cooling and heating conductivity curves are nearly coincident (Figures S23 and S24), suggesting good stability and conductivity durability. Power XRD confirms that the structure of **1** does not change after the proton conductivity measurement (Figure S25). Via linear fits of the temperature-dependent conductivity profiles using the Arrhenius equation (Figure 4d), the activation energy (*E*_a) of **1** at 98% RH is calculated to be 0.24 eV. This suggests that the Grotthuss mechanism (which typically has an *E*_a below 0.40 eV) dominates proton conduction in this compound.⁴⁶ The high proton conductivity and low activation energy should be attributed to the presence of rich H₂O molecules, terminal oxygen atoms, and counter cations within the structure of **1**, which help formation of hydrogen-bonded proton “hopping” networks.^{27,30}

CONCLUSIONS

In summary, a new 240-nuclearity polymolybdate cage **1**·g with a regular pentagonal dodecahedral geometry and accessible nanosized cavity has been synthesized for the first time. Compound **1**·g has been fully structurally characterized, and its assembly from 20 tritopic and 30 ditopic polymolybdate SBBs has been rationalized. To our knowledge, **1**·g is thus far the highest nuclearity hollow opening pentagonal dodecahedral cage with a well-defined crystal structure. Cage **1** has high stability in solution and can be regarded a new member of the giant POM cage family. The proton conductivity of **1**·g was also studied in detail. This compound exhibits superlative proton conductivity at both room temperature and high temperature and high relative humidity, representing one of the best POM-based proton conductors. This work may shed some light on the design and synthesis of hollow opening polyhedral cages using versatile POMs as building blocks. Interestingly, after the formation of

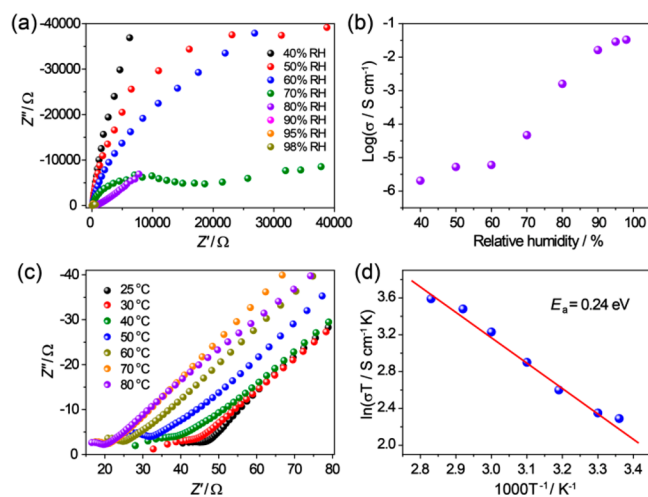


Figure 4. (a) Nyquist curves of **1**·g at 25 °C and various relative humidities. (b) Humidity-dependent proton conductivity at 25 °C. (c) Nyquist curves measured at various temperatures and 98% relative humidity. (d) Arrhenius plot of the proton conductivity of **1**·g.

tetrabutylammonium salt (TBA-1), the solubility of this giant POM cage in common organic solvents can be well improved. We expect to explore more solution properties and application of this compound in further work.

■ ASSOCIATED CONTENT

Supporting Information

The Supporting Information is available free of charge at <https://pubs.acs.org/doi/10.1021/jacs.0c06582>.

Synthesis, characterization, crystal structure, and proton conductivity properties of 1: power XRD, FT-IR, Raman spectrum, XPS, TGA, water uptake, STEM and TEM images, and proton conductivity (PDF)

Mo without squeeze treatment (CIF)

Mo squeeze treated (CIF)

■ AUTHOR INFORMATION

Corresponding Authors

Shiping Yang – The Key Laboratory of Resource Chemistry of Ministry of Education, Shanghai Key Laboratory of Rare Earth Functional Materials, Shanghai Normal University, Shanghai 200234, P. R. China; orcid.org/0000-0001-7527-4581; Email: shipingy@shnu.edu.cn

Jiang Liu – Jiangsu Collaborative Innovation Centre of Biomedical Functional Materials, School of Chemistry and Materials Science, Nanjing Normal University, Nanjing 210023, P. R. China; Email: liuj@njnu.edu.cn

Ya-Qian Lan – School of Chemistry, South China Normal University, Guangzhou 510006, P. R. China; Jiangsu Collaborative Innovation Centre of Biomedical Functional Materials, School of Chemistry and Materials Science, Nanjing Normal University, Nanjing 210023, P. R. China; orcid.org/0000-0002-2140-7980; Email: yqlan@njnu.edu.cn

Authors

Jiaomin Lin – The Key Laboratory of Resource Chemistry of Ministry of Education, Shanghai Key Laboratory of Rare Earth Functional Materials, Shanghai Normal University, Shanghai 200234, P. R. China

Ning Li – School of Chemistry, South China Normal University, Guangzhou 510006, P. R. China; School of Chemistry and Chemical Engineering, Yangzhou University, Yangzhou, Jiangsu 225002, P. R. China

Mingjie Jia – The Key Laboratory of Resource Chemistry of Ministry of Education, Shanghai Key Laboratory of Rare Earth Functional Materials, Shanghai Normal University, Shanghai 200234, P. R. China

Xiao-Min Li – Jiangsu Collaborative Innovation Centre of Biomedical Functional Materials, School of Chemistry and Materials Science, Nanjing Normal University, Nanjing 210023, P. R. China

Lu An – The Key Laboratory of Resource Chemistry of Ministry of Education, Shanghai Key Laboratory of Rare Earth Functional Materials, Shanghai Normal University, Shanghai 200234, P. R. China; orcid.org/0000-0002-6696-1651

Qiwei Tian – The Key Laboratory of Resource Chemistry of Ministry of Education, Shanghai Key Laboratory of Rare Earth Functional Materials, Shanghai Normal University, Shanghai 200234, P. R. China; orcid.org/0000-0002-4709-7378

Long-Zhang Dong – Jiangsu Collaborative Innovation Centre of Biomedical Functional Materials, School of Chemistry and

Materials Science, Nanjing Normal University, Nanjing 210023, P. R. China; orcid.org/0000-0002-9276-5101

Complete contact information is available at:

<https://pubs.acs.org/doi/10.1021/jacs.0c06582>

Author Contributions

#J.L. and N.L. contributed equally

Notes

The authors declare no competing financial interest.

■ ACKNOWLEDGMENTS

This work was partially supported by the National Natural Science Foundation of China (Nos. 21701111, 91959105, 21622104, 21701085, 21871141, and 21871142), Shanghai Sailing Program (17YF1413700), Ministry of Education of China (PCSIRT_IRT_16R49), International Joint Laboratory on Resource Chemistry (IJLRC), the NSF of Jiangsu Province of China (No. BK20171032), and Priority Academic Program Development of Jiangsu Higher Education Institutions and the Foundation of Jiangsu Collaborative Innovation Center of Biomedical Functional Materials.

■ REFERENCES

- (1) Seidel, S. R.; Stang, P. J. High-Symmetry Coordination Cages via Self-Assembly. *Acc. Chem. Res.* **2002**, *35*, 972.
- (2) Harris, K.; Fujita, D.; Fujita, M. Giant Hollow M_nL_{2n} Spherical Complexes: Structure, Functionalisation and Applications. *Chem. Commun.* **2013**, *49*, 6703.
- (3) Tranchemontagne, D. J.; Ni, Z.; O'Keeffe, M.; Yaghi, O. M. Reticular Chemistry of Metal–Organic Polyhedra. *Angew. Chem., Int. Ed.* **2008**, *47*, 5136.
- (4) Cook, T. R.; Stang, P. J. Recent Developments in the Preparation and Chemistry of Metallacycles and Metallacages via Coordination. *Chem. Rev.* **2015**, *115*, 7001.
- (5) Sun, Y.; Chen, C.; Liu, J.; Stang, P. J. Recent Developments in The Construction and Applications of Platinum-Based Metallacycles and Metallacages via Coordination. *Chem. Soc. Rev.* **2020**, *49*, 3889.
- (6) Zhang, Y.; Gan, H.; Qin, C.; Wang, X.; Su, Z.; Zaworotko, M. J. Self-Assembly of Goldberg Polyhedra from a Concave $[W_5O_{11}(CO_3)_2(SO_4)]^{3-}$ Building Block with 5-Fold Symmetry. *J. Am. Chem. Soc.* **2018**, *140*, 17365.
- (7) Zhai, Q.-G.; Mao, C.; Zhao, X.; Lin, Q.; Bu, F.; Chen, X.; Bu, X.; Feng, P. Cooperative Crystallization of Heterometallic Indium–Chromium Metal–Organic Polyhedra and Their Fast Proton Conductivity. *Angew. Chem., Int. Ed.* **2015**, *54*, 7886.
- (8) Liu, W.-J.; Yu, G.; Zhang, M.; Li, R.-H.; Dong, L.-Z.; Zhao, H.-S.; Chen, Y.-J.; Xin, Z.-F.; Li, S.-L.; Lan, Y.-Q. Investigation of the Enhanced Lithium Battery Storage in a Polyoxometalate Model: From Solid Spheres to Hollow Balls. *Small Methods* **2018**, *2*, 1800154.
- (9) Olenyuk, B.; Levin, M. D.; Whiteford, J. A.; Shield, J. E.; Stang, P. J. Self-Assembly of Nanoscopic Dodecahedra from 50 Predesigned Components. *J. Am. Chem. Soc.* **1999**, *121*, 10434.
- (10) Sigmon, G. E.; Ling, J.; Unruh, D. K.; Moore-Shay, L.; Ward, M.; Weaver, B.; Burns, P. C. Uranyl–Peroxide Interactions Favor Nanocluster Self-Assembly. *J. Am. Chem. Soc.* **2009**, *131*, 16648.
- (11) Lin, Y.; Massa, W.; Dehnen, S. Zeoball[®] $[Sn_{36}Ge_{24}Se_{132}]^{24-}$: A Molecular Anion with Zeolite-Related Composition and Spherical Shape. *J. Am. Chem. Soc.* **2012**, *134*, 4497.
- (12) Pasquale, S.; Sattin, S.; Escudero-Adán, E. C.; Martínez-Belmonte, M.; de Mendoza, J. Giant Regular Polyhedra from Calixarene Carboxylates and Uranyl. *Nat. Commun.* **2012**, *3*, 785.
- (13) Luo, D.; Wang, X.-Z.; Yang, C.; Zhou, X.-P.; Li, D. Self-Assembly of Chiral Metal–Organic Tetartoid. *J. Am. Chem. Soc.* **2018**, *140*, 118.

- (14) Long, D.-L.; Tsunashima, R.; Cronin, L. Polyoxometalates: Building Blocks for Functional Nanoscale Systems. *Angew. Chem., Int. Ed.* **2010**, *49*, 1736.
- (15) Müller, A.; Gouzerh, P. From Linking of Metal-Oxide Building Blocks in a Dynamic Library to Aiant Clusters with Unique Properties and Towards Adaptive Chemistry. *Chem. Soc. Rev.* **2012**, *41*, 7431.
- (16) Miras, H. N.; Yan, J.; Long, D.-L.; Cronin, L. Engineering Polyoxometalates With Emergent Properties. *Chem. Soc. Rev.* **2012**, *41*, 7403.
- (17) Zheng, S.-T.; Zhang, J.; Li, X.-X.; Fang, W.-H.; Yang, G.-Y. Cubic Polyoxometalate–Organic Molecular Cage. *J. Am. Chem. Soc.* **2010**, *132*, 15102.
- (18) Li, C.; Mizuno, N.; Yamaguchi, K.; Suzuki, K. Self-Assembly of Anionic Polyoxometalate–Organic Architectures Based on Lacunary Phosphomolybdates and Pyridyl Ligands. *J. Am. Chem. Soc.* **2019**, *141*, 7687.
- (19) Gao, M.-Y.; Wang, F.; Gu, Z.-G.; Zhang, D.-X.; Zhang, L.; Zhang, J. Fullerene-like Polyoxotitanium Cage with High Solution Stability. *J. Am. Chem. Soc.* **2016**, *138*, 2556.
- (20) Müller, A.; Beckmann, E.; Bögge, H.; Schmidtman, M.; Dress, A. Inorganic Chemistry Goes Protein Size: A Mo_{368} Nano-Hedgehog Initiating Nanochemistry by Symmetry Breaking. *Angew. Chem., Int. Ed.* **2002**, *41*, 1162.
- (21) Müller, A.; Shah, S. Q. N.; Bögge, H.; Schmidtman, M. Molecular Growth from a Mo_{176} to a Mo_{248} Cluster. *Nature* **1999**, *397*, 48.
- (22) Müller, A.; Krickemeyer, E.; Bögge, H.; Schmidtman, M.; Peters, F. Organizational Forms of Matter: An Inorganic Super Fullerene and Keplerate Based on Molybdenum Oxide. *Angew. Chem., Int. Ed.* **1998**, *37*, 3359.
- (23) Sigmon, G. E.; Unruh, D. K.; Ling, J.; Weaver, B.; Ward, M.; Pressprich, L.; Simonetti, A.; Burns, P. C. Symmetry versus Minimal Pentagonal Adjacencies in Uranium-Based Polyoxometalate Fullerene Topologies. *Angew. Chem., Int. Ed.* **2009**, *48*, 2737.
- (24) Bannani, F.; Floquet, S.; Leclerc-Laronze, N.; Haouas, M.; Taulelle, F.; Marrot, J.; Kögerler, P.; Cadot, E. Cubic Box versus Spheroidal Capsule Built from Defect and Intact Pentagonal Units. *J. Am. Chem. Soc.* **2012**, *134*, 19342.
- (25) Kopilevich, S.; Müller, A.; Weinstock, I. A. Amplified Rate Acceleration by Simultaneous Up-Regulation of Multiple Active Sites in an Endo-Functionalized Porous Capsule. *J. Am. Chem. Soc.* **2015**, *137*, 12740.
- (26) Schäffer, C.; Bögge, H.; Merca, A.; Weinstock, I. A.; Rehder, D.; Haupt, E. T. K.; Müller, A. A Spherical 24 Butyrate Aggregate with a Hydrophobic Cavity in a Capsule with Flexible Pores: Confinement Effects and Uptake–Release Equilibria at Elevated Temperatures. *Angew. Chem., Int. Ed.* **2009**, *48*, 8051.
- (27) Liu, W.-J.; Dong, L.-Z.; Li, R.-H.; Chen, Y.-J.; Sun, S.-N.; Li, S.-L.; Lan, Y.-Q. Different Protonic Species Affecting Proton Conductivity in Hollow Spherulike Polyoxometalates. *ACS Appl. Mater. Interfaces* **2019**, *11*, 7030.
- (28) Rezaeifard, A.; Haddad, R.; Jafarpour, M.; Hakimi, M. Catalytic Epoxidation Activity of Keplerate Polyoxomolybdate Nanoball toward Aqueous Suspension of Olefins under Mild Aerobic Conditions. *J. Am. Chem. Soc.* **2013**, *135*, 10036.
- (29) Yang, P.; Alsufyani, M.; Emwas, A.-H.; Chen, C.; Khashab, N. M. Lewis Acid Guests in a $\{\text{P}_8\text{W}_{48}\}$ Archetypal Polyoxotungstate Host: Enhanced Proton Conductivity via Metal-Oxo Cluster within Cluster Assemblies. *Angew. Chem., Int. Ed.* **2018**, *57*, 13046.
- (30) Meng, X.; Wang, H.-N.; Song, S.-Y.; Zhang, H.-J. Proton-Conducting Crystalline Porous Materials. *Chem. Soc. Rev.* **2017**, *46*, 464.
- (31) Chand, S.; Elahi, S. M.; Pal, A.; Das, M. C. Metal–Organic Frameworks and Other Crystalline Materials for Ultrahigh Superprotonic Conductivities of 10^{-2} S cm^{-1} or Higher. *Chem. - Eur. J.* **2019**, *25*, 6259.
- (32) Yang, L.; Ma, P.; Zhou, Z.; Wang, J.; Niu, J. A Crown-Shaped 24-Molybdate Cluster Constructed by Organotriphosphonate Ligand. *Inorg. Chem.* **2013**, *52*, 8285.
- (33) Gao, Q.; Wang, X.-L.; Xu, J.; Bu, X.-H. The First Demonstration of the Gyroid in a Polyoxometalate-Based Open Framework with High Proton Conductivity. *Chem. - Eur. J.* **2016**, *22*, 9082.
- (34) Li, Z.; Lin, L.-D.; Yu, H.; Li, X.-X.; Zheng, S.-T. All-Inorganic Ionic Porous Material Based on Giant Spherical Polyoxometalates Containing Core-Shell $\text{K}_6\text{@K}_{36}$ -Water Cage. *Angew. Chem., Int. Ed.* **2018**, *57*, 15777.
- (35) Liu, J.-C.; Han, Q.; Chen, L.-J.; Zhao, J.-W.; Streb, C.; Song, Y.-F. Aggregation of Giant Cerium–Bismuth Tungstate Clusters into a 3D Porous Framework with High Proton Conductivity. *Angew. Chem., Int. Ed.* **2018**, *57*, 8416.
- (36) Kong, X.-J.; Long, L.-S.; Zheng, Z.; Huang, R.-B.; Zheng, L.-S. Keeping the Ball Rolling: Fullerene-like Molecular Clusters. *Acc. Chem. Res.* **2010**, *43*, 201.
- (37) GUO, B. C.; KERNS, K. P.; CASTLEMAN, A. W. Ti8C_{12}^{+} -Metallo-Carbohedrenes: A New Class of Molecular Clusters? *Science* **1992**, *255*, 1411.
- (38) Zhang, Z.-M.; Yao, S.; Li, Y.-G.; Han, X.-B.; Su, Z.-M.; Wang, Z.-S.; Wang, E.-B. Inorganic Crown Ethers: Sulfate-Based Preyssler Polyoxometalates. *Chem. - Eur. J.* **2012**, *18*, 9184.
- (39) Tsunashima, R.; Long, D.-L.; Endo, T.; Noro, S.-i.; Akutagawa, T.; Nakamura, T.; Cabrera, R. Q.; McMillan, P. F.; Kögerler, P.; Cronin, L. Exploring The Thermochromism of Sulfite-Embedded Polyoxometalate Capsules. *Phys. Chem. Chem. Phys.* **2011**, *13*, 7295.
- (40) Schäffer, C.; Merca, A.; Bögge, H.; Todea, A. M.; Kistler, M. L.; Liu, T.; Thouvenot, R.; Gouzerh, P.; Müller, A. Unprecedented and Differently Applicable Pentagonal Units in a Dynamic Library: A Keplerate of the Type $\{(W)W_5\}_{12}\{\text{Mo}_2\}_{30}$. *Angew. Chem., Int. Ed.* **2009**, *48*, 149.
- (41) Qin, J.-S.; Du, D.-Y.; Guan, W.; Bo, X.-J.; Li, Y.-F.; Guo, L.-P.; Su, Z.-M.; Wang, Y.-Y.; Lan, Y.-Q.; Zhou, H.-C. Ultrastable Polymolybdate-Based Metal–Organic Frameworks as Highly Active Electrocatalysts for Hydrogen Generation from Water. *J. Am. Chem. Soc.* **2015**, *137*, 7169.
- (42) Chen, W.; Zhang, G.; Li, D.; Ma, S.; Wang, B.; Jiang, X. Preparation of Nitrogen-Doped Porous Carbon from Waste Polyurethane Foam by Hydrothermal Carbonization for H_2S Adsorption. *Ind. Eng. Chem. Res.* **2020**, *59*, 7447.
- (43) Tauson, V. L.; Goettlicher, J.; Sapozhnikov, A. N.; Mangold, S.; Lustenberg, E. E. Sulphur Speciation in Lazurite-Type Minerals $(\text{Na,Ca})_8\text{Al}_6\text{Si}_6\text{O}_{24}(\text{SO}_4)_2$ and Their Annealing Products: a Comparative XPS and XAS Study. *Eur. J. Mineral.* **2012**, *24*, 133.
- (44) Wang, H.-N.; Meng, X.; Dong, L.-Z.; Chen, Y.; Li, S.-L.; Lan, Y.-Q. Coordination Polymer-Based Conductive Materials: Ionic Conductivity vs. Electronic Conductivity. *J. Mater. Chem. A* **2019**, *7*, 24059.
- (45) Yang, F.; Xu, G.; Dou, Y.; Wang, B.; Zhang, H.; Wu, H.; Zhou, W.; Li, J.-R.; Chen, B. A Flexible Metal–Organic Framework With a High Density of Sulfonic Acid Sites For Proton Conduction. *Nat. Energy* **2017**, *2*, 877.
- (46) Kim, S.; Joarder, B.; Hurd, J. A.; Zhang, J.; Dawson, K. W.; Gelfand, B. S.; Wong, N. E.; Shimizu, G. K. H. Achieving Superprotonic Conduction in Metal–Organic Frameworks through Iterative Design Advances. *J. Am. Chem. Soc.* **2018**, *140*, 1077.
- (47) Li, X.-M.; Liu, J.; Zhao, C.; Zhou, J.-L.; Zhao, L.; Li, S.-L.; Lan, Y.-Q. Strategic Hierarchical Improvement of Superprotonic Conductivity in a Stable Metal–Organic Framework System. *J. Mater. Chem. A* **2019**, *7*, 25165.
- (48) Yang, Y.; He, X.; Zhang, P.; Andaloussi, Y. H.; Zhang, H.; Jiang, Z.; Chen, Y.; Ma, S.; Cheng, P.; Zhang, Z. Combined Intrinsic and Extrinsic Proton Conduction in Robust Covalent Organic Frameworks for Hydrogen Fuel Cell Applications. *Angew. Chem., Int. Ed.* **2020**, *59*, 3678.